Ultrashort Single-Wall Carbon Nanotubes Reveal Field-Emission Coulomb Blockade and Highest Electron-Source Brightness

A. Pascale-Hamri, S. Perisanu,[*] A. Derouet, C. Journet,[†] P. Vincent, A. Ayari, and S. T. Purcell

ILM, Université Claude Bernard Lyon 1 et CNRS, UMR 5586, F-69622 Villeurbanne, France
(Received 18 December 2013; published 26 March 2014)

We present here well-defined Coulomb staircases using an original field-emission experiment on several individual *in situ*—grown single-wall carbon nanotubes. A unique *in situ* process was applied nine times to progressively shorten one single-wall carbon nanotube down to $\simeq 10$ nm, which increased the oscillations periods from 5.5 to 80 V, the temperature for observable Coulomb staircase to 1100 K and the currents to 1.8 μA. This process led to the brightest electron source ever reported [9×10^{11} A/(str m^2 V)].

The Coulomb blockade (CB) has been and continues to be studied intensively for its interest in fundamental physics and technology [1–7]. Two important limitations of CB devices [5] are low operating currents, now reported up to $\simeq 10^{-7}$ A [3], and poor room temperature performance. The later has been improved over the years by fabricating ever smaller structures, in particular when the Coulomb island is a single-wall carbon nanotube (SWCNT) [6–9]. Hybrid single-electron transistors (SETs) have been proposed for higher currents [10].

The operating current and temperature of a specific device can be understood from the physics of the CB. The simplest CB device has one electrically insulated island sandwiched between two tunnel junctions and is powered by a dc voltage source V. The CB usually manifests itself by first blocking the current at low V while at higher V; though less often observed, the current increases by steps forming a Coulomb staircase (CS) with each step corresponding to the presence of one additional electron on the island [1,6,11–13]. An original device that can cast a new light on CB phenomena is one based on field emission (FE), where the most resistive junction is the classic vacuum triangular barrier for which the concept of electron tunneling was invented [14]. Though not yet demonstrated experimentally, this geometry has recently been analyzed theoretically [15] and should lead to particular voltage current characteristics due to the high asymmetry of the two junctions, such as extremely large voltages needed for bringing an additional electron on the island (ΔV) and thus addition energies, defined by $E_{\mathrm{add}} \equiv e\Delta V$ with e the electron charge [5]. Evidence of a CS for a standard symmetrical SET device for which the solid-state tunneling is in the FE regime was recently demonstrated at low temperature [16]. A vacuum FE CB device, as well as being a new geometry for the CB in general, could create an original on-demand electron source for advanced experiments in vacuum nanoelectronics, such as Hanbury Brown–Twiss based antibunching [17] or vacuum

analogues to solid-state single-electron sources [18] of interest for quantum computing [19,20]. A key parameter for electron sources is the reduced brightness, which can be defined as $B_r = I/(\Omega A V)$ [21], where I is the FE current, A the source area, and Ω the solid angle of emission.

The CB depends on the interplay of three energies. First, there is the charging energy when an electron arrives on the island, which is mostly of electrostatic nature [5,7,22]: $E_E \simeq e^2/C$, with C the total capacitance of the island with respect to its environment [5]. The second is the driving voltage energy $E_V = eV$. Third, the thermal energy $E_T = k_B T$ must be taken into account since the electrons on the island are in contact with electrodes at a temperature T. As V is varied, the CB usually manifests itself by first blocking the current for $E_V < E_E$. In SETs, the CB creates a specific diamondlike structure in the current characteristics as a function of source and gate voltages [2–4,7,23,24]. As T is varied, the CB disappears progressively when E_T becomes greater than $E_E \propto 1/C$. This led quite quickly to the fabrication of a commercial thermometer working down to a few milliKelvin [25]. Furthermore, CB devices were optimized to reach room temperature operation by shrinking the device size, and hence its capacitance down to $C \simeq 1$ aF, which gives $E_E \gtrsim E_T \approx 25$ meV [26,27].

We report in this Letter in-depth observations of CS on three different SWCNT cantilevers denoted SWCNT1–3. A schematic of the experiments is shown in Fig. 1(a). SWCNTs were grown *in situ* on etched tungsten tips during FE on which were first deposited sequentially an amorphous carbon layer by pyrolyse and a Ni catalyst overlayer by evaporation, as described in detail in a previous work [28]. Upon application of a voltage to the support tip, a high electric field develops at the apex of the SWCNT, which induces a FE tunneling current. The support tips are mounted on calibrated heating loops, which allow variable temperature experiments. A carbon layer deposited on the tip prior to the growth electrically insulated the SWCNT island, ensuring thus CB behavior, as shown on Fig. 1(b)
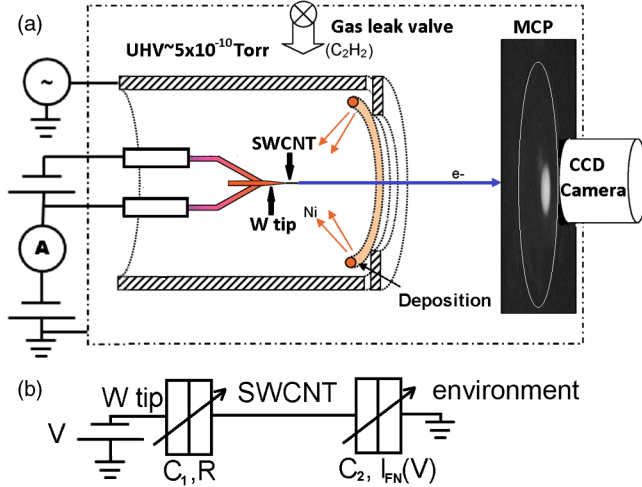
FIG. 1 (color online). (a) Schematic of our experimental setup. The SWCNT is grown *in situ* on an etched *W* tip placed inside a UHV chamber. The *W* tip is mounted on a heating loop supplied by a battery that can be floated up to several kiloVolt. The FE electrons form an image on the phosphor screen placed in front of a CCD camera, after being multiplied by a micro-channel plate (MCP). (b) Equivalent circuit in FE. The SWCNT is insulated from the *W* tip by an amorphous carbon layer and emits electrons in the vacuum. The capacitance C_1 (C_2) is taken between the SWCNT and the *W* tip (the rest of the environment, respectively).

FIG. 2 (color online). Observations of the CB for SWCNTs. (a) Fowler Nordheim (FN) plot of the experimental FE $I(V)$ at $T = 300$ K for SWCNT1 (filled circle) and fit with strong apex curvature FN formula (-) (S.2 in Supplemental Material). (b) Difference between two successive current values normalized to their average for the data of (a). Strong CS oscillations are present. (c) Mechanical eigenfrequency $f(V)$ for SWCNT3 (filled circle) at $T = 300$ K and fit (-) with its theoretical prediction [29]. High-frequency impedance miss-matching in our system prevents obtaining the curve over the whole voltage range available for FE. (d) For SWCNT3, relative difference between the mechanical $f(V)$ experimental points and fit for SWCNT3 presented in (c) (filled circle) compared with the relative difference between the FE current and the corrected FN fit (squares) measured simultaneously. Both oscillations have the same voltage period and functional form. The mechanical curve had to be multiplied a factor ×50 to fall on the current curve.

(S.1 in Supplemental Material). Furthermore, SWCNT3 was controllably shortened *in situ* nine times by current-induced shortening (CIS). Each new length was estimated by either the mechanical eigenfrequency [29] for the first two lengths or by comparison of experimental and simulated electrical capacitances for all the lengths. These simulations were based on CS theory for the FE configuration [15] and electrostatic calculations of surface charge for our specific geometry, as presented in S.3 (Supplemental Material).

The voltage dependence of the FE current, $I(V)$, for SWCNT1 at room temperature is presented in Fig. 2(a) in the standard FE representation $\ln(I/V^2)$ as a function of $1/V$. The remarkable new feature is that this $I(V)$ shows systematic deviations from standard tunneling theory with a very well-defined periodicity of 8.5 V, as presented in Fig. 2(b) (S.2 in Supplemental Material). Such oscillations were equally observed up to 600 K for SWCNT2 and for SWCNT3, as presented on Fig. 2(d) for SWCNT3.

Furthermore, applying an additional ac voltage to the surrounding cylindrical anode can excite flexural mechanical vibrations when the driving frequency matches one of the cantilever's eigenfrequencies [30]. Vibrations can be detected either by the increase in size of the FE pattern [31] or by the change in the FE current [32] when sweeping the frequency through resonance (S.3 in Supplemental Material). As well, when the SWCNT is brought to negative voltage for FE, the accumulated electrical charge induces longitudinal stress on the SWCNT that strongly increases the eigenfrequencies [32], similar to the tuning of a guitar

string (S.2 in Supplemental Material). The dependence of the eigenfrequency on the applied voltage for SWCNT3, $f(V)$, is presented in Fig. 2(c) at room temperature. At first sight, there is very good agreement with the fit based on theoretical predictions of tuning [29]. However, a similar comparison between the experimental data and the fit as done previously for $I(V)$ shows the same systematic and periodic deviations with the same voltage period of about 5.5 V for SWCNT3 [Fig. 2(d)]. As discussed hereafter and in S.3 (Supplemental Material), these oscillations in $f(V)$ are due to the change in electrostatic tuning induced by the residence of individual additional electrons on the SWCNT. This phenomenon was previously observed on SWCNT bridges in the transistor configuration, but only for $T < 4$ K [8,9].

A unique experiment of CIS allowed us to modify the CS in a predictable way and thus unambiguously determine its origin. As shown in Figs. 3(a) and 3(b), the oscillation period was progressively increased from 5.5 to $\simeq 80$ V as SWCNT3 was shortened. Note that an extrapolation of the oscillations to $V = 0$ V indicates that the minimum additional charge on the sample measurable in this FE configuration was decreased from about $33e$ to about $7e$ during the shortening. Next, the maximum temperature for which
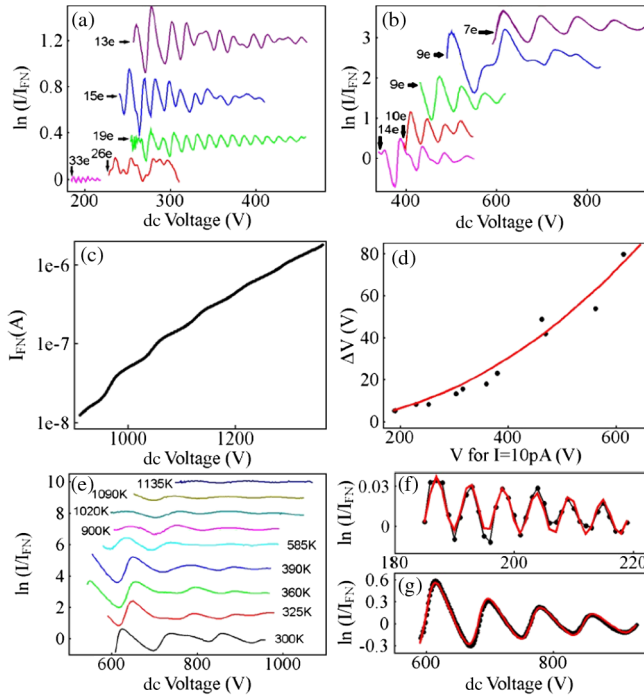
FIG. 3 (color online). Evolution of CB as a function of length and temperature for SWCNT3. (a) and (b) Experimental CS as we decrease the length, with the FN dependence in the absence of CS subtracted and vertically shifted for better readability. Voltage periods were from bottom to top: 5.5, 8.5, 13.6, 16, 20, 25, 38, 49, 54, and 80 V, and we can also clearly see an increase of the oscillation amplitude. For some shortening stages, with periods of 8.5, 25, and 54 V, multiple periodicities are observed, perhaps due to electron-electron interactions. (c) Experimental $I(V)$ curve for the shortest length of SWCNT3 with CS oscillations up to $I = 1.8$ μA. (d) Experimental points for the voltage periodicity as a function of the voltage necessary for $I = 10$ pA (squares) as we decrease the SWCNT's length. Fit gives an electric field $F = 11$ V/nm at the apex (S.2 and S.3 in Supplemental Material). (e) Experimental temperature dependence of CS oscillations for the last stage of shortening up to $T \simeq 1100$ K, presented like in (a) and (b) with temperature-independent period of oscillation, as predicted by theory [15]. (f) and (g) Measured CB oscillations (solid line with dots) are in very good quantitative agreement with a fit to theory [15] (solid line), as presented for the longest (f) and the shortest (g) length (S.3 in Supplemental Material).

the CS was observed increased progressively from $\simeq$600 K to $\simeq$1100 K, and the maximum current allowing the CB observation rose from about 100 nA up to 1.8 μA; the shortest length $I(V)$ curve is presented in Fig. 3(c). Stable currents above the CS detection limit were observed up to 5 μA for emission half angles of $\simeq$1.5°, which we used for calculating the brightness. The progressive disappearance of the CS oscillations with temperature is presented in Fig. 3(e) for the shortest length of SWCNT3.

Let us now compare these results with theoretical predictions. The electrostatic energy of the system at constant voltage is $E_E = (e^2/2C)(n - C_2V/e)^2 + \text{const}$ [15], with n the number of additional electrons, C_1 the

capacitance between the SWCNT and the tungsten tip, C_2 the capacitance of the SWCNT with respect to the rest of its environment (anodes, phosphor screen, etc.), and $C = C_1 + C_2$ [see Fig. 1(b)]. At thermal equilibrium, the state with lowest energy has the highest probability, which occurs when $n \simeq C_2V/e$ giving the experimental period $\Delta V = e/C_2$ as the difference between the voltages of the states with $n + 1$ and n electrons. Electron level spacing due to confinement in the SWCNT is negligible compared to ΔV, as discussed in [7] and in S.3 (Supplemental Material). From Figs. 3(a) and 3(b), C_2 is found to be in the extremely low range of 2–30 zF, as we decrease the SWCNT's length. Though more complicated to obtain, C_1 is found by fitting the experimental CS oscillations with the theoretical $I(V)$ (S.3 in Supplemental Material). Such a fit is shown in Figs. 3(f) and 3(g) and gives for SWCNT3 C_1 in the range of 466 zF to 1.26 aF, depending on the SWCNT's length, and the insulating layer resistance $R \simeq 200$ kΩ, which largely exceeds the quantum unit of resistance $h/4e^2 \simeq 6.5$ kΩ necessary for the CB [5].

Going further, we used these capacitances and $f(V)$ to determine the geometrical dimensions of interest. We have neglected the quantum and the amorphous carbon layer contributions to the capacitances, as discussed in S.3 (Supplemental Material). The values found were $t = 1$ nm for the amorphous carbon layer, $r = 0.78$ nm for the radius, and $L_0 = 63.5$ nm for the initial length of SWCNT3. After the first shortening, a length of $L_1 = 48$ nm was determined. These simulations are consistent with a final SWCNT3 length of $\simeq$10 nm, which is $\simeq L_0/6$ (S.3 in Supplemental Material). Note that the value of r gives a source area $A = 1.9$ nm^2, which is used to calculate the source brightness (see below). A strong confirmation of the validity of our approach is the fitting of the period as a function of voltage necessary for $I = 10$ pA for each length [Fig. 3(d)]. This fit gives us the electric field $F = 11$ V/nm necessary for a $I_{FN} = 10$ pA. This higher than usual value, which is length independent according to the FE theory, can be explained by the extremely small emitting surface. Furthermore, as $F \propto V$ for a given SWCNT length, we can infer that the maximum field we applied to our SWCNT was $\simeq$28 V/nm. Electric fields higher than 30 V/nm were used for controlled CIS at temperatures of roughly 2000 K, still largely inferior to the 103 V/nm measured as the field necessary to extract atoms from crystalline carbon structures at 20 K [33].

Contrary to most experiments found in literature where $C_1 \simeq C_2$, here we have $C_1 \simeq 100C_2$ due to the very weak coupling of the SWCNT with its environment other than the tip. The extremely small value of C_2 leads to very large CS periods of up to $\Delta V = 80$ V, which is 2 to 4 orders of magnitude larger than values found in the literature and which, according to Likharev's definition [5], is the addition energy per unit charge E_{add}/e. This asymmetry also explains why in our experiment the voltage period in

the I-V curve ΔV (5.5 to 80 V) is not directly related to the charging energy $E_E \simeq e^2/(2C_1)$ (60 to 170 meV) since $C_1 \gg C_2$ and $n - C_2 V/e \lesssim 1$. The temperature where the CB oscillations should disappear is $T_C \simeq E_E/k_B \simeq e^2/(2Ck_B) = 1955$ K. Note that at 1100 K the oscillations are still easily observable Fig. 3e). Higher temperatures were not explored for fear of losing the nanotube due to desorption assisted by the high electric field.

To our knowledge, these are the only CB oscillations observed above room temperature. In the first instance, this is due to our high values of E_E, related to the small size of the SWCNT but also to the fact that it is not in contact with a dielectric medium. Higher values of E_E have recently been reported in a SET structure for currents measured through an insulating channel formed by current induced degradation of a graphene flake [24]; however, it is difficult to draw a comparison to this work as only the first plateau was observed and not oscillations.

The commonly achieved highest currents for CB oscillations are in the range of some tens of nA mostly limited by the onset of direct current from the source to the drain. In contrast, these FE experiments give CB oscillations already up to 1.8 μA, as presented in Fig. 3(c). This geometry has strongly enhanced emission from the SWCNT apex because the vertical orientation of the nanotube generates large field enhancement factors at the apex $\simeq L/r \simeq 10 - 100$. In addition here, the covalent bonds between carbon atoms make the island robust against electromigration and breakdown.

These SWCNTs can be proved to be the brightest electron sources described in the literature. Using the definition for reduced brightness B_r, as defined in the first paragraph, and $I = 5$ μA, a half angle of the emission cone of 1.5°, $V = 1500$ V and $r = 0.78$ nm one gets $B_r = 9 \times 10^{11}$ A/(str m^2 V), some 100 times higher than the highest previously reported value [34]. These characteristics open immediate possibilities in vacuum electronics such as for better electron microscope sources.

Let us draw several remarks in conclusion. First, these highest reported values of operating temperature, current, and brightness open perspectives for higher performance CB applications. Addition energies on the order of 100 $k_B T$ were proposed as a reasonable limit to exclude temperature assisted electron tunneling through the barriers, which is a bottleneck for memory storage devices [5]. Second, we are proceeding to measure the energy spectra of the emitted electrons, which should give a direct measurement of e/C, the voltage drops across the SWCNT, and its apex temperature [35], allowing thus valid modeling of the electrothermal problem, including the ballistic character of the SWCNT phonon and electron transport. Finally, this FE CB emitter is a new type of electron source that brings together mesoscopic physics and FE of which there are few examples. As a start, it should arguably have less Poissonian emission statistics and furthermore may open a route toward

more coherent [18] and brighter single-electron emitters for ultrafast electron diffraction spectroscopy of molecular structural dynamics with atomic resolution [36].

[*]sorin.perisanu@univ-lyon1.fr
[†]Present address: LMI, Université Lyon 1 et CNRS, France.

[1] T. A. Fulton and G. J. Dolan, Phys. Rev. Lett. **59**, 109 (1987).
[2] P. Jarillo-Herrero, S. Sapmaz, C. Dekker, L. P. Kouwenhoven, and H. S. J. van der Zant, Nature (London) **429**, 389 (2004).
[3] S. J. Shin, J. J. Lee, H. J. Kang, J. B. Choi, S.-R. Eric Yang, Y. Takahashi, and D. G. Hasko, Nano Lett. **11**, 1591 (2011).
[4] J. P. Cleuziou, W. Wernsdorfer, V. Bouchiat, T. Ondarcuhu, and M. Monthioux, Nat. Nanotechnol. **1**, 53 (2006).
[5] K. K. Likharev, IEEE Proc. **87**, 606 (1999).
[6] H. W. C. Postma, T. Teepen, Z. Yao, M. Grifoni, and C. Dekker, Science **293**, 76 (2001).
[7] M. Bockrath, D. H. Cobden, P. L. McEuen, N. G. Chopra, A. Zettl, A. Thess, and R. E. Smalley, Science **275**, 1922 (1997).
[8] B. Lassagne, Y. Tarakanov, J. Kinaret, D. Garcia-Sanchez, and A. Bachtold, Science **325**, 1107 (2009).
[9] G. A. Steele, A. K. Hüttel, B. Witkamp, M. Poot, H. B. Meerwaldt, L. P. Kouwenhoven, and H. S. J. van der Zant, Science **325**, 1103 (2009).
[10] A. M. Ionescu, S. Mahapatra, and V. Pott, IEEE Electron Device Lett. **25**, 411 (2004).
[11] R. P. Andres, S. Datta, M. Dorogi, J. Gomez, J. I. Henderson, B. Janes, V. R. Kolagunta, C. P. Kubiak, W. Mahoney, R. F. Osifchin, R. Reifenberger, M. P. Samanta, and W. Tian, J. Vac. Sci. Technol. A **14**, 1178 (1996).
[12] C. Dubuc, J. Beauvais, and D. Drouin, Appl. Phys. Lett. **90**, 113104 (2007).
[13] E. A. Speets, B. Dordi, B. J. Ravoo, N. Oncel, A. Hallbäck, H. J. W. Zandvliet, B. Poelsema, G. Rijnders, D. H. A. Blank, and D. N. Reinhoudt, Small **1**, 395 (2005).
[14] R. Fowler and L. W. Nordheim, Proc. R. Soc. A **119**, 173 (1928).
[15] O. E. Raichev, Phys. Rev. B **73**, 195328 (2006).
[16] C. Kim, H. S. Kim, H. Qin, and R. H. Blick, Nano Lett. **10**, 615 (2010).
[17] H. Kiesel, A. Renz, and F. Hasselbach, Nature (London) **418**, 392 (2002).
[18] G. Féve, A. Mahé, J.-M. Berroir, T. Kontos, B. Placais, D. C. Glattli, A. Cavanna, B. Etienne, and Y. Jin, Science **316**, 1169 (2007).
[19] S. Hermelin, S. Takada, M. Yamamoto, S. Tarucha, A. D. Wieck, L. Saminadayar, C. Bäuerle, and T. Meunier, Nature (London) **477**, 435 (2011).
[20] R. P. G. McNeil, M. Kataoka, C. J. B. Ford, C. H. W. Barnes, D. Anderson, G. A. C. Jones, I. Farrer, and D. A. Ritchie, Nature (London) **477**, 439 (2011).

[21] N. de Jonge, Y. Lamy, K. Schoots, and T. H. Oosterkamp, Nature (London) **420**, 393 (2002).

[22] R. Saito, M. Fujita, G. Dresselhaus, and M. S. Dresselhaus, Appl. Phys. Lett. **60**, 2204 (1992).

[23] C. Kim, M. Prada, and R. H. Blick, ACS Nano **6**, 651 (2012).

[24] A. Barreiro, H. S. J. van der Zant, and L. M. K. Vandersypen, Nano Lett. **12**, 6096 (2012).

[25] S. Farhangfar, K. P. Hirvi, J. P. Kauppinen, J. P. Pekola, J. J. Toppari, D. V. Averin, and A. N. Korotkov, J. Low Temp. Phys. **108**, 191 (1997).

[26] K. Matsumoto, M. Ishii, K. Segawa, Y. Oka, B. J. Vartanian, and J. S. Harris, Appl. Phys. Lett. **68**, 34 (1996).

[27] J. B. Cui, M. Burghard, and K. Kern, Nano Lett. **2**, 117 (2002).

[28] M. Marchand, C. Journet, D. Guillot, J. M. Benoit, B. I. Yakobson, and S. T. Purcell, Nano Lett. **9**, 2961 (2009).

[29] S. Perisanu, V. Gouttenoire, P. Vincent, A. Ayari, M. Choueib, M. Bechelany, D. Cornu, and S. T. Purcell, Phys. Rev. B **77**, 165434 (2008).

[30] P. Poncharal, Z. L. Wang, D. Ugarte, and W. A. de Heer, Science **283**, 1513 (1999).

[31] S. Perisanu, P. Vincent, A. Ayari, M. Choueib, M. Bechelany, D. Cornu, P. Miele, and S. T. Purcell, Phys. Status Solidi A **204**, 1645 (2007).

[32] S. T. Purcell, P. Vincent, C. Journet, and V. T. Binh, Phys. Rev. Lett. **89**, 276103 (2002).

[33] M. K. Miller and G. D. W. Smith, *Atom Probe Microanalysis: Principles and Applications to Material Problems* (Materials Research Society, Pittsburgh, 1989).

[34] N. deJonge, M. Allioux, J. T. Oostveen, K. B. K. Teo, W. I. Milne, Phys. Rev. Lett. **94**, 186807 (2005).

[35] S. T. Purcell, P. Vincent, C. Journet, and V. Thien Binh, Phys. Rev. Lett. **88**, 105502 (2002).

[36] M. Gao, C. Lu, H. Jean-Ruel, L. C. Liu, A. Marx, K. Onda, S. Koshihara, Y. Nakano, X. Shao, T. Hiramatsu, G. Saito, H. Yamochi, R. R. Cooney, G. Moriena, G. Sciaini, and R. J. Dwayne Miller, Nature (London) **496**, 343, 343 (2013).

[37] See Supplemental Material at http://link.aps.org/supplemental/10.1103/PhysRevLett.112.126805 for additionnal information about the SWCNT growth and shortening (S.1), Field Emission in CB regime (S.2) and Capacitance Simulations and fitting (S.3) can be found here.